

TESTING THE MAGNETAR MODEL VIA LATE TIME RADIO OBSERVATIONS OF TWO MACRONOVA CANDIDATES

ASSAF HORESH¹, KENTA HOTOKEZAKA², TSVI PIRAN², EHUD NAKAR³, PAUL HANCOCK^{4,5}

Draft version June 22, 2021

ABSTRACT

Compact binary mergers may have already been observed as they are the leading model for short gamma-ray bursts (sGRBs). Radioactive decay within the ejecta from these mergers is expected to produce an infra-red flare, dubbed macronova (or kilonova), on a time scale of a week. Recently two such macronova candidates were identified in followup observations of sGRBs, strengthening the possibility that those indeed arise from mergers. The same ejecta will also produce a long term (months to years) radio emission due to its interaction with the surrounding ISM. In search for this emission, we observed the two macronova candidates, GRB 130603B and GRB 060614 with the Jansky very large array (VLA) and the Australia Telescope Compact Array (ATCA). Our observations resulted in null-detections, putting strong upper limits on the kinetic energy and mass of the ejecta. A possible outcome of a merger is a highly magnetized neutron star (a magnetar), which has been suggested as the central engine for GRBs. Such a magnetar will deposit a significant fraction of its energy into the ejecta leading to a brighter radio flare. Our results, therefore, rule out magnetars in these two events.

1. INTRODUCTION

The coalescence of two compact objects such as a Neutron Star (ns) - Black Hole (BH) merger or a ns² merger has been a leading candidate for the progenitor system for short-duration (< 2s) Gamma-ray bursts (sGRBs; Eichler et al. 1989; Narayan, Paczynski & Piran 1992; see reviews by Nakar 2007, Berger 2014). Li & Paczynski (1998) suggested that mergers will be accompanied by the so called “macronova” (or “kilonova”). They suggested that the radioactive decay of the neutron rich matter ejected in a merger event would lead to a brief (~ 1 day) optical signal that might be detectable. More recently, Barnes & Kasen (2013) and Tanaka & Hotokezaka (2013) have revised the original prediction of Li & Paczynski. As the optical depth for r-process elements is high, the optical signal is expected to be mostly absorbed, and a longer (~ 1 week) IR signal is expected instead.

A second prediction of the merger scenario is of late-time radio emission (Nakar & Piran 2011). The same ejecta that produce the macronova is expected to interact with the interstellar medium (ISM). The resulting shockwave, ploughing through the ISM will accelerate

electrons and produce magnetic fields. In turn, this will lead to synchrotron radio emission, similar to the process responsible for radio emission from supernovae (e.g., Chevalier 1982; Chevalier & Fransson 2006) or GRB afterglows (Sari 1997; Sari et al. 1999). The rise time and the peak flux of this radio flare, depend mainly on the ejecta mass, its velocity and on the density of the ISM. For a macronova ejecta mass of $M_{ej} \sim 0.01 M_{\odot}$ and velocity range of $v_{ej} \sim 0.1 - 0.3 c$, as predicted by recent numerical simulations (Rosswog et al. 2013; Hotokezaka et al. 2013, Bauswein et al. 2013), the radio emission is expected to rise over a time-scale of months to years.

A variant of the simple merger scenario, motivated by a strong amplification of magnetic fields at the merger shown in numerical simulations (Price & Rosswog 2006, Rezzolla 2012, Giacomazzo & Perna 2013, Giacomazzo et al. 2015, Kiuchi et al. 2015), is the magnetar scenario, in which the remnant of the merger is a highly magnetized ns with a period of ~ 1 ms and a large magnetic field of $B > 10^{13}$ G (Usov 1992; Rosswog & Davies 2002; Bucciantini et al. 2012; Fan et al. 2013; Giacomazzo et al. 2013; Metzger & Piro 2014; Siegel et al. 2015). The magnetar has been suggested (e.g., Usov 1992; Duncan & Thompson 1992; Zhang & Mészáros 2001; Metzger 2010) as the central engine that powers GRBs. In this scenario, the magnetar deposits most of its rotational energy, as it spins down, in the macronova ejecta, accelerating it to high relativistic velocities, thus significantly enhancing the expected radio flare signal. A magnetar with a ~ 1 ms period deposits a kinetic energy of $\approx 3 \times 10^{52}$ erg. The time-scale and the peak flux of the expected radio emission in this case, can be calculated (in a simplistic way; see §3) according to the

¹ Benoziyo Center for Astrophysics, Weizmann Institute of Science, 76100 Rehovot, Israel

² Racah Institute of Physics, The Hebrew University, Jerusalem 91904, Israel

³ Raymond and Beverly Sackler School of Physics & Astronomy, Tel Aviv University, Tel Aviv 69978, Israel

⁴ International Centre for Radio Astronomy Research (ICRAR), Curtin University, GPO Box U1987, Perth WA 6845, Australia

⁵ ARC Centre of Excellence for All-Sky Astrophysics (CAAS-TRO)

formalism of Nakar & Piran (2011), but with a high relativistic velocity ($\beta \equiv v_{ej}/c \approx 1$). The magnetar radio emission, that will also rise over a long time scale, is expected to be brighter by a few orders of magnitude than the non-magnetar merger scenario (as first discussed by Metzger & Bower 2013; see §5). In addition to the bright radio emission from the forward shock, there may be additional radio emission from the pulsar wind nebula, which is expected to peak over much shorter time scales (see Piro & Kulkarni 2013; Metzger & Piro 2014).

Berger et al. (2013) and Tanvir et al. (2013) have identified a macronova candidate associated with GRB 130603B. The macronova signal was detected, as predicted, in the IR band and it lasted less than 30 days⁶. Berger et al. (2013) find that an ejecta with a mass of $M_{ej} = 0.05 - 0.08 M_{\odot}$ and velocities of $v_{ej} \approx 0.1 - 0.3 c$ is needed⁷ to produce the observed signal. A second macronova candidate associated with the earlier event GRB 060614, has been recently discovered by Yang et al. (2015) who re-examined the data obtained with the Hubble Space Telescope and found excess emission at the F814W band (see also Jin et al. 2015). Yang et al. find that it can be explained by a macronova with a significantly more massive ejecta, $M_{ej} = 0.03 - 0.1 M_{\odot}$, with velocities of $v_{ej} \approx 0.1 - 0.2 c$.

In search for a late-time radio emission, originating from a forward shock in the ISM, as predicted by Nakar & Piran (2011), we obtained late-time radio observations of both GRB 130603B and GRB 060614. In the next section we briefly describe the radio observations. In §3 we provide details about how the predictions of the radio signal are calculated. We compare our predictions with the results of our observations in §4, and briefly summarize in §5.

2. RADIO OBSERVATIONS

2.1. VLA observations of GRB 130603B

We observed GRB 130603B with the Karl G. Jansky Very Large Array (VLA), in B configuration, on 2015, February 12 UT ($T_0 + 619$ days). The observation was performed at central frequency of 3 GHz using J1120+1420 and 3C286 as phase and flux calibrators, respectively. We analysed the data using standard AIPS⁸ and CASA⁹ routines. We found no significant radio emission at the position of the GRB with a 3σ detection limit of $60 \mu\text{Jy}$.

At early times, GRB 130603B was observed with the VLA by Fong et al. (2014). They detected radio emission a few hours after the GRB was discovered. This

⁶ HST observations detected the IR source 9 days after the sGRB was detected. A second observing HST epoch undertaken 21 days later revealed that the source have faded away (Tanvir et al. 2013)

⁷ Note that a wider range of ejecta mass and velocities is consistent with the data.

⁸ Astronomical Image Processing System

⁹ Common Astronomy Software Applications package; McMullin et al. 2007

emission was rapidly fading away below the detection limit, within four days as expected from a typical GRB afterglow. An observation at day 84 after discovery (Fong et al., 2014) resulted in a null-detection of $34 \mu\text{Jy}$ (3σ) at 6.7 GHz.

2.2. ATCA observations of GRB 060614

We used the Australia Telescope Compact Array (ATCA) to observe GRB 060614A at 2.1 GHz on 2015 May 9 UT ($T_0 + 337$ days). The following calibrator sources: PKS B1921–293 (band-pass), PKS B1934–638 (flux), and PKS B2213–45 (phase) were used. The data were processed using MIRIAD (Sault, Teuben & Wright 1995). The resulting image achieved an RMS noise of $50 \mu\text{Jy}$ at the location of the GRB, however no detection was made with a 3σ upper limit of $150 \mu\text{Jy}$.

3. PREDICTION OF THE MAGNETAR SIGNAL

The interaction of the ejected mass with the ISM leads to a late time (months-years) radio signal. The luminosity of the signal and the peak time depend both on the properties of the ejecta and of the ISM. At high frequencies the signal is expected to peak once the ejecta starts to decelerate. This will occur when the ejecta ploughed through sufficient ISM mass to slow it down, i.e., comparable to the ejecta mass. The deceleration radius and time, and the peak radio flux are then simply defined by Nakar & Piran (2011).

In the magnetar scenario, the stable ns remnant formed in a binary ns merger is expected to have a typical rotational period of $P \sim 1$ ms. The rotational energy of the ns is

$$E_{\text{rot}} = \frac{I(2\pi)^2}{2P^2} \quad (1)$$

where I is the moment of inertia. For the above period, the rotational energy is $\approx 3 \times 10^{52}$ erg. Depositing this additional energy into an ejecta mass of $10^{-2} M_{\odot}$ will result in a relativistic outflow, leading to a stronger radio signal at late times. It is important to stress that our estimates are sensitive just to the magnetar period and not to its magnetic field. The total rotational energy of the magnetar is released and deposited in the ejecta on a time scale much shorter than the time scales that we consider here.

Adopting the above typical magnetar energy and assuming the ejecta mass and ISM density, the predicted radio light curves can be calculated using the Nakar & Piran (2011) formalism (see also Piran et al. 2013). However, there are two additional points that need to be treated more carefully. First, the peak flux is given assuming that the observed frequency is above the self-absorbed frequency. Second, Nakar & Piran address the case of non-relativistic ejecta and thus neglected relativistic effects.

The major relativistic effects on the observed flux are: (i) relativistic time effects, (ii) the Doppler shift, and

(iii) relativistic beaming¹⁰ (see e.g. Piran 2004 for a review). These effects play important roles depending on the initial Lorentz factor. Roughly speaking, an observer will measure a brighter flux than those expected from Newtonian motion until the blast wave has sufficiently decelerated. The deceleration timescale, in the relativistic case, is shorter than the Newtonian one by a factor of $\Gamma^{-8/3}$. The synchrotron frequency ν_m corresponding to γ_m ¹¹ decreases with time. For an observed frequency ν that was initially below ν_m the flux peaks when $\nu = \nu_m$ at:

$$t_{\text{peak}} = 120 \text{ days} \left(\frac{E}{3 \cdot 10^{52}} \right)^{1/3} \left(\frac{\epsilon_e}{0.1} \right)^{4/3} \left(\frac{\epsilon_B}{0.1} \right)^{1/3} \left(\frac{\nu}{3 \text{ GHz}} \right)^{-2/3}. \quad (2)$$

where, E is the energy deposited in the ejecta, ϵ_B and ϵ_e are the shock equipartition parameters of the magnetic field and electron energy, respectively. The peak flux at this time is

$$F_{\nu, \text{peak}} = 8 \text{ mJy} \left(\frac{E}{3 \cdot 10^{52}} \right) \left(\frac{\epsilon_B}{0.1} \right)^{1/2} \left(\frac{n}{0.1 \text{ cm}^{-3}} \right)^{1/2} \left(\frac{D}{10^{28} \text{ cm}} \right)^{-2}, \quad (3)$$

where D is the distance to the source, and n is the ISM density. The above estimates are valid when synchrotron self-absorption is negligible. The radio frequencies are often below the self-absorption frequency ν_a . For $\nu_m < \nu < \nu_a$ the peak time (after the deceleration) is when $\nu = \nu_a$:

$$t_{\text{peak}} = 170 \text{ days} \left(\frac{E}{3 \cdot 10^{52}} \right)^{\frac{p+2}{3p+2}} \left(\frac{\epsilon_e}{0.1} \right)^{\frac{4(p-1)}{3p+2}} \left(\frac{n}{0.1 \text{ cm}^{-3}} \right)^{\frac{4}{3p+2}} \left(\frac{\epsilon_B}{0.1} \right)^{\frac{p+2}{3p+2}} \left(\frac{\nu}{3 \text{ GHz}} \right)^{\frac{-2(p+4)}{3p+2}}, \quad (4)$$

and the peak flux is estimated as

$$F_{\nu, \text{peak}} = 5 \text{ mJy} \left(\frac{E}{3 \cdot 10^{52}} \right)^{\frac{2p+3}{3p+2}} \left(\frac{\epsilon_e}{0.1} \right)^{\frac{5(p-1)}{3p+2}} \left(\frac{n}{0.1 \text{ cm}^{-3}} \right)^{\frac{8-3p}{6p+4}} \left(\frac{\epsilon_B}{0.1} \right)^{\frac{p+4}{6p+4}} \left(\frac{\nu}{3 \text{ GHz}} \right)^{\frac{5p-5}{3p+2}} \left(\frac{D}{10^{28} \text{ cm}} \right)^{-2}. \quad (5)$$

In order to account for the blast wave dynamics in both relativistic and non-relativistic regime, we follow

¹⁰ In the case of an isotropic ejecta, the relativistic beaming does not change the total luminosity.

¹¹ We have assumed that the electrons are accelerated by the blast-wave with a power-law energy distribution of $N_e \sim \gamma_e^{-p}$, with some minimum Lorentz factor γ_m .

the numerical procedures of Hotokezaka & Piran (2015). Note, that we do not use directly the approximate equations above, but perform a full numerical calculation. In short (see the following references for more details), the blast wave expansion is determined by conservation of energy of the ejecta and swept-up material as $M(R)(\Gamma\beta c)^2 = E$, in a similar way to Piran et al. (2013). Here $M(R)$ is the sum of the ejecta mass and the mass of the swept-up ISM at a radius R . For a given blast-wave dynamics we calculate the synchrotron radiation, using the fluid velocities and energy density just behind the shock. Then, at each observer time, we sum up the emission from each fluid element following Eq. (4) of Granot, Sari, & Piran 1999a. This includes all relativistic propagation effects consistently and reproduces the light curves of Sari et al. (1998) in the ultra-relativistic limit and of Nakar & Piran (2011) in the non-relativistic limit. To account for synchrotron self-absorption, we calculated the absorption coefficients based on Granot, Piran, & Sari (1999b). In addition, throughout our calculations, we adopt the following parameter values: $\epsilon_e = 0.1$ and $p = 2.5$.

Next, we calculate (following Hotokezaka & Piran 2015) the expected radio flare signature, using a range of values for E , and n . We repeat the calculations using two distinct values for the microphysical parameter, ϵ_B , i.e., $\epsilon_B = 0.1$ and $\epsilon_B = 0.01$. The expected radio signal was calculated for each of the macronova candidates, separately, at the frequencies in which they were observed. Our predictions of the radio signals are presented in Figure 1.

Figure 2 shows examples of radio light curves specifically for the fiducial magnetar model with an energy of $E = 3 \times 10^{52}$ erg and ejecta mass of $M_{\text{ej}} = 0.01, 0.1 M_{\odot}$ for various ISM density values. The relativistic effects alone shorten the peak time, compared to the Newtonian case, by a factor of ~ 20 (for $\Gamma = 3$). Adding the effect of synchrotron-self absorption, however, prolongs the peak time. Thus, the combined effect of synchrotron self absorption and relativistic motion on the peak time is only a factor of a few, compared to the Newtonian case. The peak flux can also vary by an order of magnitude. If we take the case of $n = 0.1$ as an example, the peak luminosity and time in the naive Newtonian case would have been $\approx 2 \times 10^{40}$ erg/s, and ≈ 930 days, compared to $\approx 4 \times 10^{41}$ erg/s, and ≈ 200 days, in the full relativistic calculation.

4. COMPARISON OF THE MAGNETAR MODEL WITH OBSERVATIONS

As seen in Figure 1, we can rule out a large fraction of the $E - n$ phase space for both GRB 130603B and GRB 060614. A main uncertainty in the determination of radio flare signals involves the external density of the ISM. The surrounding circumburst density is typically determined from analysis of the GRB's afterglow. However, this determination typically suffers from numerous uncertainties and degeneracies between

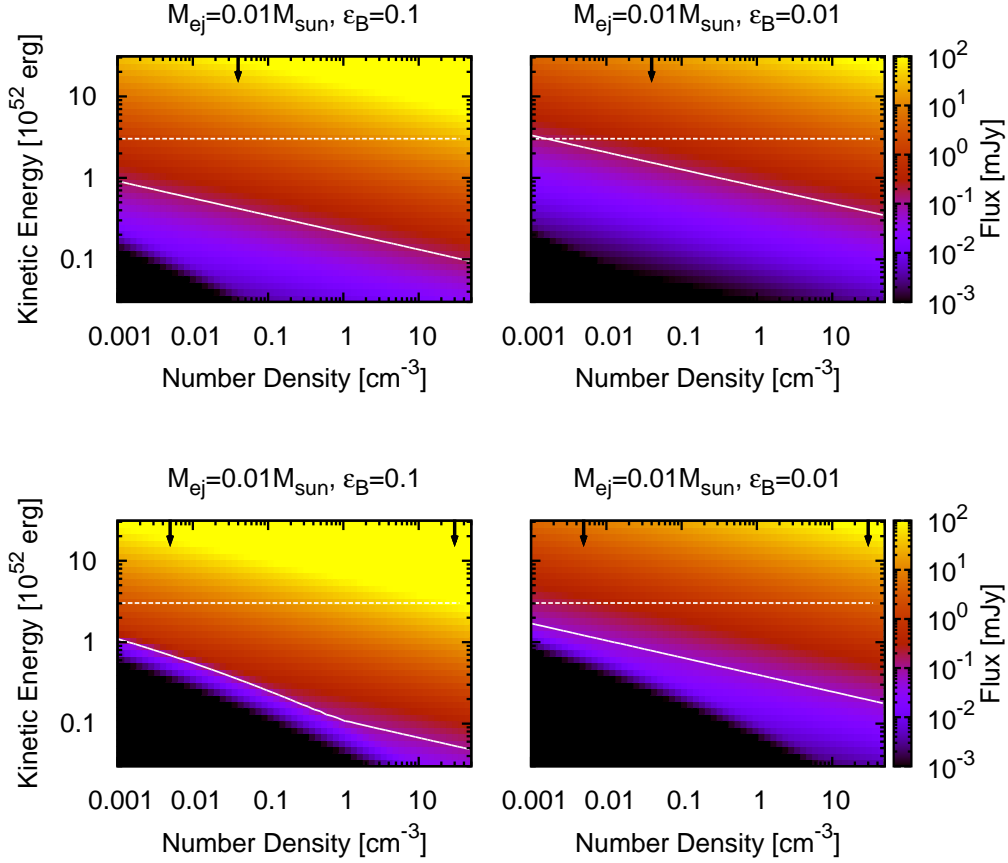


FIG. 1.— Predictions of the radio flux from a macronova (including the magnetar model). The predictions are for the macronova candidates GRB 060614 (top panel) and GRB 130603B (bottom panel) at the times we performed our radio observations (see §2 for details). The radio flux of each event is calculated for a different combination of the kinetic energy and ISM density. We assume here the fiducial value of the ejecta mass in the magnetar model of $M_{\text{ej}} = 0.01 M_{\odot}$. We also assume $\epsilon_e = 0.1$ and use both $\epsilon_B = 0.1$ (left panel) and $\epsilon_B = 0.01$ (right panel). The dashed white line represent the fiducial value of the kinetic energy in the magnetar model, $E_k = 3 \times 10^{52}$ erg. The solid white lines represent our observational limits. The arrows represent the ISM density value (or value range) measured based on the observed afterglow properties (see §4).

this density and other afterglow parameters (in particular with ϵ_B). For example, Fong et al. (2014) analyzed X-ray, optical and radio observations of the afterglow of GRB 130603B. They find that the possible circumburst density ranges from 0.005 to 30 cm^{-3} . This large range of uncertainty demonstrates the difficulty in estimating the density even when afterglow information is available in three bands. Xu et al. (2009) have analyzed the afterglow of GRB 060614. They find that a density of 0.04 cm^{-3} is consistent with the data but they do not try to bracket it. The range of values of the ISM densities for both GRB 130603B and GRB 060614 are within the range that we have discussed here, and are both sufficiently large to rule out the canonical magnetar model.

In light of the uncertainty in the ISM density and the microphysical parameters, we present in Figure 3 different areas in the $M_{\text{ej}} - E$ phase space that can be

ruled out for various ISM density and ϵ_B values. This large phase space, as in Figure 1, accounts not only for the magnetar scenario (discussed below) but also for the cases where there is no additional energy injection such as the “standard” non-relativistic macronova scenario presented in Nakar & Piran (2011).

Assuming that a magnetar output energy is $3 \times 10^{52} \text{ erg}$, then even for a very low ISM density $n = 0.001 \text{ cm}^{-3}$ and for a relatively low energy conversion of shockwave energy to magnetic fields, $\epsilon_B \sim 0.01$, the expected radio signal at the time of our radio observations for both events are above our detection limits. Given that we did not detect any radio emission, this rules out the fiducial magnetar model for macronova events associated with GRBs.

It is worth mentioning that the above conclusion is based on the assumption of spherical symmetry. Devia-

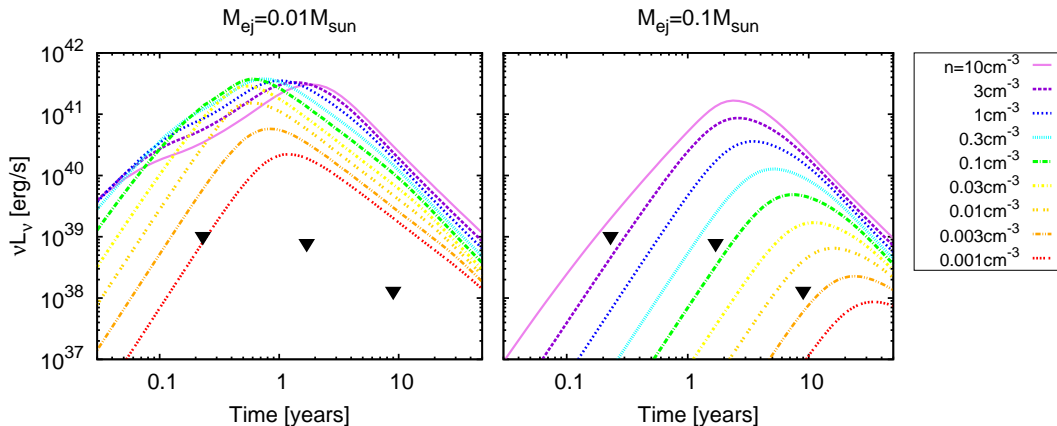


FIG. 2.— Predicted radio light curves in the magnetar scenario when both relativistic effects and synchrotron self-absorption are included. The light curves are calculated assuming kinetic energy of $E_k = 3 \times 10^{52}$ erg and a range of ISM densities (see legend). Solid triangles represent the late-time radio observations (see § 2).

tions from spherical symmetry, that are expected, would reduce somewhat the signal and delay the peak time (Margalit & Piran, 2015). However this amounts only to about 10% difference in peak luminosity and a factor of ~ 2 in peak time. We cannot rule out a magnetar with a large mass ejection ($> 0.1 M_\odot$), in low density environment, by the absence of radio emission. The velocity of this large ejecta mass will be non-relativistic and is expected to produce weak emission below our detection limits (Figure 2). Other cases where the radio emission can be highly suppressed is an even more extreme case, where a minute amount of energy is converted in the shock to magnetic fields, i.e., $\epsilon_B \ll 0.001$. Atypical high ISM density will also lead to a suppression of the radio signal as the optical depth will increase.

5. SUMMARY

Compact binary mergers are expected to be followed by a macronova emission and long-lasting radio emission. In this paper we have searched for this radio signal including the one which is predicted specifically by the magnetar scenario. In this latter case, a merger results in highly magnetized ns that deposits energy into a small amount of ejecta mass that becomes relativistic. If this relativistic ejecta interacts with an ISM that is not too dilute, it is expected to produce a bright radio emission which will peak over time scales of months to years.

Our search was focused on two GRBs (GRB 130603B & GRB 060614) that were the first to exhibit a macronova-like emission, thus indicating the ejection of a small amount of mass, a condition needed for the late production of a radio flare. Therefore, we have observed these GRB positions at late times with the VLA and the ATCA telescopes. Our radio observations resulted in null-detections. Comparing the predicted radio emis-

sion with our upper limits, we can rule out a wide range of kinetic energies, ejecta masses, ISM densities and microphysical parameters. As shown in Figures 1, 2, and 3, the range of parameters we rule out includes the canonical magnetar model.

A previous search for magnetar radio emission from sGRBs has been performed by Metzger & Bower (2013). They observed 7 sGRBs within 1 – 3 years after discovery with the VLA but did not detect any emission. They used their non-detections to constrain the merger magnetar scenario as well. However, their work is different from ours in several ways. First, they have used the Newtonian calculations following Nakar & Piran (2011) but with $\beta = 0.8$ and kinetic energy of 3×10^{52} erg/s. Thus, they have not accounted for relativistic effects and did not explore a wide range of ejecta masses. Given these limitations and the lower observational sensitivities (due to the old capabilities of the VLA), Metzger & Bower (2013) only ruled out magnetar scenarios with densities above $n = 0.03 \text{ cm}^{-3}$. Our observed sample is also different since the sGRBs that we observed have been associated with macronova emission, previously not observed in other sGRBs.

As discussed above, our conclusion is limited by several factors. While, we use a wide range of values for the model parameters, there are still extreme parameters under which the magnetar model is consistent with our observations. This includes, extremely high (or low) ISM density, extremely low values (< 0.001) of ϵ_B , and extremely small ejecta mass. Given these limitations and the fact that we studied only two macronova events, provides further motivation to undertake a large campaign of carefully designed late-time radio observations of sGRBs.

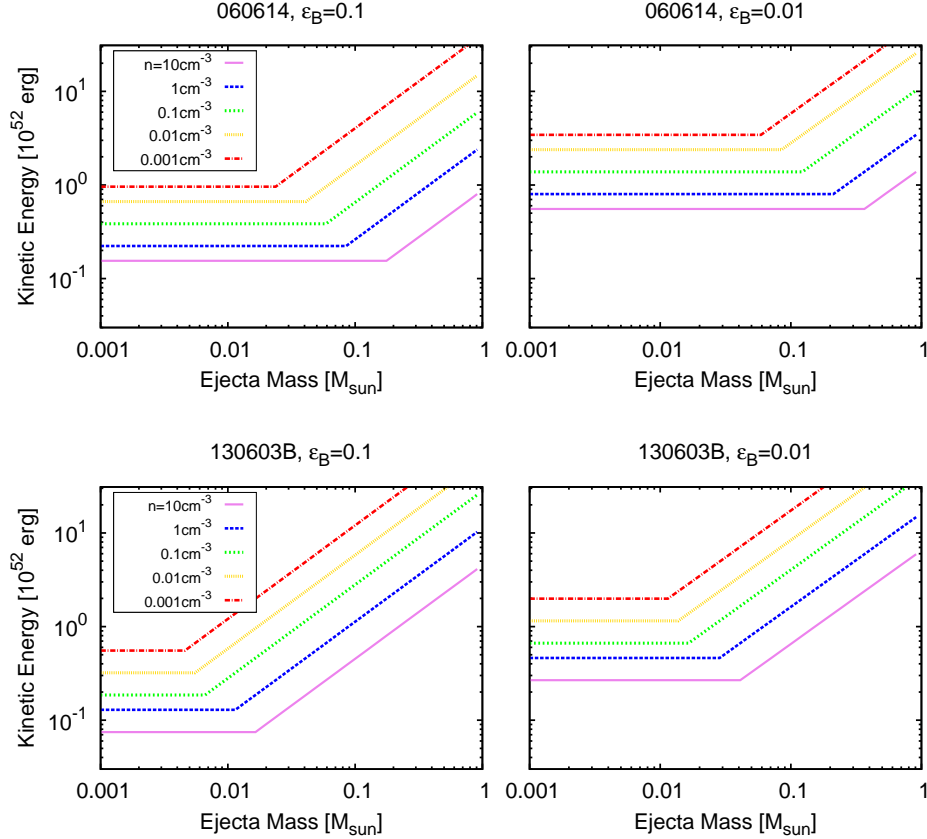


FIG. 3.— The allowed phase space of energy and ejecta mass (including the magnetar and non-magnetar scenario) of the two macronovae candidates GRB 060614 (top panel) and GRB 130603B (bottom panel). The allowed phase space for different ISM density values (different line colors) is below each density line. The allowed phase space is based on our late-time radio observations. We also assume $\epsilon_e = 0.1$ and use both $\epsilon_B = 0.1$ (left panel) and $\epsilon_B = 0.01$ (right panel).

ACKNOWLEDGMENTS

We thank the ATCA and the VLA staff for promptly scheduling the observation of these targets of opportunity. The National Radio Astronomy Observatory is a facility of the National Science Foundation operated under cooperative agreement by Associated Universities, Inc. Research leading to these results has received

funding from the EU/FP7 via ERC grant 307260; ISF, Minerva, and Weizmann-UK grants; as well as the I-Core Program of the Planning and Budgeting Committee and the Israel Science Foundation, and the Israel Space Agency. Parts of this research were conducted by the Australian Research Council Centre of Excellence for All-sky Astrophysics (CAASTRO), through project number CE110001020.

REFERENCES

- Barnes J., Kasen D., 2013, *ApJ*, 775, 18
 Bauswein A., Goriely S., Janka H.-T., 2013, *ApJ*, 773, 78
 Berger E., Fong W., Chornock R., 2013, *ApJ*, 774, L23
 Berger E., 2014, *ARA&A*, 52, 43
 Bucciantini N., Metzger B. D., Thompson T. A., Quataert E., 2012, *MNRAS*, 419, 1537
 Chevalier R. A., 1982, *ApJ*, 259, 302
 Chevalier R. A., Fransson C., 2006, *ApJ*, 651, 381
 Duncan R. C., Thompson C., 1992, *ApJ*, 392, L9
 Eichler D., Livio M., Piran T., Schramm D. N., 1989, *Natur*, 340, 126
 Fan Y.-Z., Yu Y.-W., Xu D., Jin Z.-P., Wu X.-F., Wei D.-M., Zhang B., 2013, *ApJ*, 779, L25
 Fong W., et al., 2014, *ApJ*, 780, 118
 Giacomazzo B., Perna R., 2013, *ApJ*, 771, L26
 Giacomazzo B., Perna R., 2013, *ApJ*, 771, L26
 Giacomazzo B., Zrake J., Duffell P. C., MacFadyen A. I., Perna R., 2015, *ApJ*, 809, 39
 Granot J., Piran T., Sari R., 1999a, *ApJ*, 513, 679
 Granot J., Piran T., Sari R., 1999b, *ApJ*, 527, 236
 Granot J., Sari R., 2002, *ApJ*, 568, 820
 Hotokezaka K., Kyutoku K., Okawa H., Shibata M., Kiuchi K., 2011, *PhRvD*, 83, 124008
 Hotokezaka K., Kyutoku K., Shibata M., 2013, *PhRvD*, 87, 044001
 Hotokezaka K., Piran T., 2015, *MNRAS*, 450, 1430
 Jin Z.-P., Li X., Cano Z., Covino S., Fan Y.-Z., Wei D.-M., 2015, *ApJ*, 811, L22
 Kiuchi K., Sekiguchi Y., Kyutoku K., Shibata M., Taniguchi K., Wada T., 2015, *PhRvD*, 92, 064034

- Li L.-X., Paczyński B., 1998, *ApJ*, 507, L59
 Margalit B., Piran T., 2015, *MNRAS*, 452, 3419
 Metzger B. D., 2010, *ASPC*, 432, 81
 Metzger B. D., Piro A. L., 2014, *MNRAS*, 439, 3916
 Metzger B. D., Bower G. C., 2014, *MNRAS*, 437, 1821
 Nakar E., 2007, *PhR*, 442, 166
 Nakar E., Piran T., 2011, *Natur*, 478, 82
 Narayan R., Paczynski B., Piran T., 1992, *ApJ*, 395, L83
 Paczynski B., 1986, *ApJ*, 308, L43
 Piran T., 2004, *RvMP*, 76, 1143
 Piro A. L., Kulkarni S. R., 2013, *ApJ*, 762, L17
 Price D. J., Rosswog S., 2006, *Sci*, 312, 719
 Rosswog S., Davies M. B., 2002, *MNRAS*, 334, 481
 Rosswog S., Piran T., Nakar E., 2013, *MNRAS*, 430, 2585
 Rezzolla L., 2012, *ASPC*, 453, 41
 Sault R. J., Teuben P. J., Wright M. C. H., 1995, *ASPC*, 77, 433
 Sari R., 1997, *ApJ*, 489, L37
 Sari R., Piran T., Narayan R., 1998, *ApJ*, 497, L17
 Siegel D. M., Ciolfi R., Rezzolla L., 2014, *ApJ*, 785, L6
 Tanaka M., Hotokezaka K., 2013, *ApJ*, 775, 113
 Tanvir N. R., Levan A. J., Fruchter A. S., Hjorth J., Hounsell R. A., Wiersema K., Tunnicliffe R. L., 2013, *Natur*, 500, 547
 Xu D., et al., 2009, *ApJ*, 696, 971
 Yang B., et al., 2015, *NatCo*, 6, 7323
 Usov V. V., 1992, *Natur*, 357, 472
 Zhang B., Mészáros P., 2001, *ApJ*, 552, L35